

# Second order functional renormalization group approach to one-dimensional systems in real and momentum space

Björn Sbierski and Christoph Karrasch

*Dahlem Center for Complex Quantum Systems and Institut für Theoretische Physik,  
Freie Universität Berlin, 14195, Berlin, Germany*

(Dated: February 5, 2022)

We devise a functional renormalization group treatment for a chain of interacting spinless fermions which is correct up to second order in the interaction strength. We treat both inhomogeneous systems in real-space as well as the translational invariant case in a k-space formalism. The strengths and shortcomings of the different schemes as well as technical details of their implementation are discussed. We use the method to study two proof-of-principle problems in the realm of Luttinger liquid physics, namely reflection at interfaces and power laws in the occupation number as a function of crystal momentum.

## I. INTRODUCTION

The functional renormalization group (fRG) is a specific realization of the RG concept on the basis of vertex functions for many-particle systems [1, 2]. The idea is to introduce an infrared cutoff  $\Lambda$  in the bare Green function of the system at hand,  $G_0 \rightarrow G_0^\Lambda$  with the limits  $G_0^{\Lambda=\infty} = 0$  and  $G_0^{\Lambda=0} = G_0$ . Beyond these requirements, the nature of this cutoff is generic and a particular choice will be presented below. Naturally, all vertices now depend on  $\Lambda$ ; the ensuing fRG flow equations quantify the change of the vertex functions with  $\Lambda$  and represent a coupled set of differential equations organized in an infinite hierarchy of Feynman diagrams. In the limit  $\Lambda = \infty$ , by virtue of the trivial dynamics, the vertex functions are known exactly. Integration of the flow equations from  $\Lambda = \infty$  to  $\Lambda = 0$  in principle yields an exact expression for the vertex functions of the underlying problem. In practice, the infinite hierarchy of flow equations has to be truncated; fRG results are then only an approximation, which, however, goes beyond perturbation theory since an infinite re-summation of Feynman diagrams is included. Further, the approximations can ensure the vertex functions to be exact up to some order  $n$  in the interaction strength, in this case we call this formalism fRG- $n$ .

While the fact that only certain types of Feynman diagrams are included in the fRG methodology is a very delicate point that requires a careful assessment of its approximate predictions on a case-by-case basis, the approach offers a range of benefits that renders it a versatile tool for a wide range of physical situations. It can be set up for vertices defined both in the Matsubara or Keldysh formalism [3–5], allowing the treatment of systems in and out of equilibrium. Unlike matrix-product state approaches [6], it is oblivious to the degree of entanglement in the system. Noninteracting parts of the system (i.e., leads) can be integrated out exactly and simply yield additional self-energy contributions for the interacting degrees of freedom. Since self-energies are

nothing but single-particle vertices, this strategy readily integrates in the fRG formalism and allows for the treatment of open systems.

In this work, we devise various second-order fRG schemes for one-dimensional spinless fermions, document their capabilities and limitations, and discuss technical details of their implementation. Our results extend previous first order fRG-1 studies which addressed transport through nanowires [7, 8] as well as Luttinger liquid power laws in the presence of impurities [9, 10] or disorder [11]. A real-space fRG-2 framework for spinful one-dimensional fermions has been established recently and featured prominently in comparison to experimental data on the 0.7-anomaly in quantum transport [12–14]. First simple attempts to devise a k-space fRG-2 scheme for the spinful Hubbard model can be found in Refs. [15] and [16]; the methods were used to compute the quasi-particle weight [15] and the ground state phase diagram [16]. In the realm of quantum impurity problems, both fRG-1 as well as full fRG-2 approaches already exist [17]. Momentum space fRG was widely used to investigate the flow of the four-point vertex for two-dimensional problems [18–21]; the complexity of these systems, however, renders it very difficult to implement true fRG-2 schemes. The key goal of this paper is to develop and benchmark second-order fRG approaches to spinless systems in real- and k-space.

Our Hamiltonian takes the form

$$H = \sum_j -t_j c_j^\dagger c_{j+1} - h.c. + U_j (n_j - \frac{1}{2})(n_{j+1} - \frac{1}{2}), \quad (1)$$

where  $c_j^\dagger$  creates a fermion at site  $j$  (we put the lattice constant to unity,  $a = 1$ ), and  $n_j = c_j^\dagger c_j$  is the number operator. We allow for a spatial dependence of the nearest neighbor hoppings  $t_j$  and interactions  $U_j$  in order to address both translationally-invariant and inhomogeneous systems. We focus on half-filling and ground state properties (i.e., equilibrium at  $T = 0$ ). The model, which is related to the XXZ-spin-1/2 chain by a Jordan-Wigner transformation, is well studied. In the homoge-

neous case, it is exactly solvable by the Bethe-Ansatz, and its low-energy physics is governed by the Luttinger liquid fixed point for  $U/t < 2$  [22]; it is generally susceptible to matrix-product state type methods like density matrix renormalization group (DMRG). The model thus represents an ideal testbed for fRG method development, which is our central goal in this paper.

In order to investigate both translationally-invariant and inhomogeneous systems, we use a Matsubara frequency cutoff (we briefly comment on results obtained via a k-space cutoff for the former case). The bare Green function  $G_0(\omega) = [i\omega - H_0]^{-1}$  with  $H_0$  representing the single-particle terms is augmented by a sharp multiplicative cutoff

$$G_0^\Lambda(\omega) = \Theta(|\omega| - \Lambda) G_0(\omega). \quad (2)$$

The paper is organized as follows: In Sec. II we develop fRG-2 in real space as applicable for the inhomogeneous model as in (1). As an application, we consider the backscattering of carriers at an abrupt junction between two different but homogeneous chains. In Sec. III we consider the homogeneous case which allows us to work in k-space. Here, we use our formalism to calculate the ground state occupation numbers and confirm Luttinger liquid power laws with exponents of second order in the interaction strength. We conclude in Sec. IV.

## II. FRG IN REAL SPACE

*fRG flow equations.* For the spinless fermion chain (1), the single-particle indices (site index, Matsubara frequency) can be summarized in a multi-index as  $1 = (j_1, \omega_1)$ . Then, the fRG flow equation for the flowing self-energy  $\Sigma^\Lambda$  reads [1]

$$\partial_\Lambda \Sigma^\Lambda(1'; 1) = - \sum_{2, 2'} S_{2, 2'}^\Lambda U^\Lambda(2' 1'; 21) \quad (3)$$

where  $S^\Lambda = G^\Lambda \left( \partial_\Lambda [G_0^\Lambda]^{-1} \right) G^\Lambda$  is the single-scale propagator, and  $G^\Lambda = [[G_0^\Lambda]^{-1} - \Sigma^\Lambda]^{-1}$ . In a truncation neglecting the 3-particle vertex (which is generated along the flow by terms of third order in the bare interaction  $v$ ), the flow equations for the 2-particle vertex  $U^\Lambda$  read [1]

$$\partial_\Lambda U_\Pi^\Lambda(1' 2'; 12) = \sum_{33' 44'} U^\Lambda(1' 2'; 34) U^\Lambda(3' 4'; 12) \quad (4)$$

$$\times [S_{33'}^\Lambda G_{44'}^\Lambda + S_{44'}^\Lambda G_{33'}^\Lambda],$$

$$\partial_\Lambda U_\Xi^\Lambda(1' 2'; 12) = \sum_{33' 44'} U^\Lambda(1' 4'; 32) U^\Lambda(3' 2'; 14) \quad (5)$$

$$\times [S_{33'}^\Lambda G_{44'}^\Lambda + S_{44'}^\Lambda G_{33'}^\Lambda],$$

$$\partial_\Lambda U_\Delta^\Lambda(1' 2'; 12) = - \sum_{33' 44'} U^\Lambda(2' 4'; 32) U^\Lambda(3' 1'; 14) \quad (6)$$

$$\times [S_{33'}^\Lambda G_{44'}^\Lambda + S_{44'}^\Lambda G_{33'}^\Lambda],$$

where we have introduced the notation

$$U^\Lambda = v + U_\Pi^\Lambda + U_\Xi^\Lambda + U_\Delta^\Lambda. \quad (7)$$

Here,  $v(1' 2'; 12)$  is the bare antisymmetric vertex, defined from the interacting Hamiltonian as  $H_I = \frac{1}{4} \sum_{1, 2, 1', 2'} v(1' 2'; 12) c_1^\dagger c_2^\dagger c_2 c_1$ . The following entries take the value  $U_j$ , independent of the frequencies (for all vertex functions, conservation of Matsubara frequency is implied)

$$\begin{aligned} & v(j, j+1; j, j+1) \\ &= v(j+1, j; j+1, j) \\ &= -v(j, j+1; j+1, j) \\ &= -v(j+1, j; j, j+1) \\ &= U_j \end{aligned} \quad (8)$$

and all  $v$ -entries of a different form vanish.

*fRG-2 scheme, general form.* The only approximation so far was to set the three-particle vertex to zero. However, the number of remaining flow equations generally scales with the fourth power of the number of interacting degrees of freedom; a full solution is therefore only possible for impurity problems [17], and further simplifications need to be devised [13] for 1d systems.

A straightforward way to set up a fRG-2 scheme is to approximate  $U^\Lambda \rightarrow v$  on the right hand side of Eqs. (4) to (6). This choice greatly simplifies the frequency dependence of  $U_{\Pi, \Xi, \Delta}^\Lambda(1' 2'; 12)$ . Each vertex depends on the correspondingly labeled composite (bosonic) Matsubara frequency

$$\Pi = \omega_{1'} + \omega_{2'} = \omega_1 + \omega_2, \quad (9)$$

$$\Xi = \omega_{2'} - \omega_1 = \omega_2 - \omega_{1'}, \quad (10)$$

$$\Delta = \omega_{1'} - \omega_1 = \omega_2 - \omega_{2'}, \quad (11)$$

respectively. Note that we explicitly used fermionic frequency conservation,  $\omega_1' + \omega_2' = \omega_1 + \omega_2$ . At first glance it seems that by inserting the bare vertex on the right hand side of Eqs. (4) to (6), one generates a large number of different index structures on the left hand side. However, it turns out that many of them are related by symmetries (time-reversal, complex-conjugation or anti-symmetry) of the vertex such as  $U_\Delta^\Lambda(1' 2'; 12) = -U_\Xi^\Lambda(2' 1'; 12)$ .

*fRG-2 scheme, tight-binding chain.* For the tight-binding chain defined in Eq. (1), the set of independent index structures is given by

$$U_{\Pi}^{\Lambda}(j_1, \Pi - \omega'; j_1 + 1, \omega'; j_2, \Pi - \omega; j_2 + 1, \omega) \equiv P_{j_1 j_2}^{++}(\Pi), \quad (12)$$

$$U_{\Xi}^{\Lambda}(j_2, \omega'; j_1, \Xi + \omega; j_1, \omega; j_2, \Xi + \omega') \equiv X_{j_1 j_2}^{00}(\Xi), \quad (13)$$

$$U_{\Xi}^{\Lambda}(j_2, \omega'; j_1 - 1, \Xi + \omega; j_1, \omega; j_2, \Xi + \omega') \equiv X_{j_1 j_2}^{0-}(\Xi), \quad (14)$$

$$U_{\Xi}^{\Lambda}(j_2 + 1, \omega'; j_1 + 1, \Xi + \omega; j_1, \omega; j_2, \Xi + \omega') \equiv X_{j_1 j_2}^{++}(\Xi), \quad (15)$$

$$U_{\Xi}^{\Lambda}(j_2 + 1, \omega'; j_1 - 1, \Xi + \omega; j_1, \omega; j_2, \Xi + \omega') \equiv X_{j_1 j_2}^{+-}(\Xi), \quad (16)$$

which can be conveniently treated as matrices depending on a single frequency. Their flow equations read

$$\partial_{\Lambda} P_{j_1 j_2}^{++}(\Pi) = T \sum_{\omega} U_{j_1} [S_{j_1 j_2}^{\Lambda}(\omega) G_{j_1+1, j_2+1}^{\Lambda}(\Pi - \omega) + S_{j_1+1, j_2+1}^{\Lambda}(\omega) G_{j_1, j_2}^{\Lambda}(\Pi - \omega) - S_{j_1+1, j_2}^{\Lambda}(\omega) G_{j_1, j_2+1}^{\Lambda}(\Pi - \omega) - S_{j_1, j_2+1}^{\Lambda}(\omega) G_{j_1+1, j_2}^{\Lambda}(\Pi - \omega)] U_{j_2}, \quad (17)$$

$$\begin{aligned} \partial_{\Lambda} X_{j_1 j_2}^{00}(\Xi) = T \sum_{\omega} [U_{j_2} U_{j_1} S_{j_2+1, j_1+1}^{\Lambda}(\omega) G_{j_1+1, j_2+1}^{\Lambda}(\omega - X) + U_{j_1-1} U_{j_2} S_{j_2+1, j_1-1}^{\Lambda}(\omega) G_{j_1-1, j_2+1}^{\Lambda}(\omega - X) \\ + U_{j_1} U_{j_2-1} S_{j_2-1, j_1+1}^{\Lambda}(\omega) G_{j_1+1, j_2-1}^{\Lambda}(\omega - X) + U_{j_1-1} U_{j_2-1} S_{j_2-1, j_1-1}^{\Lambda}(\omega) G_{j_1-1, j_2-1}^{\Lambda}(\omega - X)] + S \leftrightarrow G, \end{aligned} \quad (18)$$

$$\begin{aligned} \partial_{\Lambda} X_{j_1 j_2}^{0-}(\Xi) = -T \sum_{\omega} [U_{j_1-1} U_{j_2} G_{j_1-1, j_2+1}^{\Lambda}(\omega - X) S_{j_2+1, j_1}^{\Lambda}(\omega) + U_{j_1-1} U_{j_2-1} G_{j_1-1, j_2-1}^{\Lambda}(\omega - X) S_{j_2-1, j_1}^{\Lambda}(\omega) \\ + U_{j_1-1} U_{j_2} S_{j_1-1, j_2+1}^{\Lambda}(\omega) G_{j_2+1, j_1}^{\Lambda}(\omega + X) + U_{j_1-1} U_{j_2-1} S_{j_1-1, j_2-1}^{\Lambda}(\omega) G_{j_2-1, j_1}^{\Lambda}(\omega + X)], \end{aligned} \quad (19)$$

$$\partial_{\Lambda} X_{j_1 j_2}^{++}(\Xi) = T \sum_{\omega} U_{j_1} (S_{j_2+1, j_1}^{\Lambda}(\omega) G_{j_1+1, j_2}^{\Lambda}(\omega - X) + S_{j_1+1, j_2}^{\Lambda}(\omega) G_{j_2+1, j_1}^{\Lambda}(\omega + X)) U_{j_2}, \quad (20)$$

$$\partial_{\Lambda} X_{j_1 j_2}^{+-}(\Xi) = T \sum_{\omega} U_{j_1-1} (S_{j_2+1, j_1}^{\Lambda}(\omega) G_{j_1-1, j_2}^{\Lambda}(\omega - X) + S_{j_1-1, j_2}^{\Lambda}(\omega) G_{j_2+1, j_1}^{\Lambda}(\omega + X)) U_{j_2}. \quad (21)$$

Expressed in terms of these quantities, the flow equation for the self-energy (3) takes the form

$$\begin{aligned} \partial_{\Lambda} \Sigma_{ij}^{\Lambda}(\nu) = T \sum_{\omega} \delta_{ij} [-U_{i-1} S_{i-1, i-1}^{\Lambda}(\omega) - U_i S_{i+1, i+1}^{\Lambda}(\omega)] + \delta_{i+1, j} U_i S_{i, j}^{\Lambda}(\omega) + \delta_{i-1, j} S_{i, j}^{\Lambda}(\omega) U_j \\ + \delta_{ij} \sum_k \left( S_{kk}^{\Lambda}(\omega) X_{kj}^{00}(0) + S_{k, k-1}^{\Lambda}(\omega) X_{kj}^{0-}(0) + S_{k, k+1}^{\Lambda}(\omega) X_{k+1, j}^{0-}(0) \right) \\ + \delta_{i, j-1} \sum_k \left( S_{kk}^{\Lambda}(\omega) X_{jk}^{0-}(0) + S_{k, k-1}^{\Lambda}(\omega) X_{k-1, j-1}^{++}(0) + S_{k, k+1}^{\Lambda}(\omega) X_{jk}^{+-}(0) \right) \\ + \delta_{i, j+1} \sum_k \left( S_{kk}^{\Lambda}(\omega) X_{j+1, k}^{0-}(0) + S_{k, k-1}^{\Lambda}(\omega) X_{kj}^{+-}(0) + S_{k, k+1}^{\Lambda}(\omega) X_{kj}^{++}(0) \right) \\ - S_{j-1, i-1}^{\Lambda}(\omega) P_{i-1, j-1}^{++}(\nu + \omega) - S_{i+1, j-1}^{\Lambda}(\omega) P_{j-1, i}^{++}(\nu + \omega) - S_{i-1, j+1}^{\Lambda}(\omega) P_{i-1, j}^{++}(\nu + \omega) \\ + S_{i+1, j+1}^{\Lambda}(\omega) P_{i, j}^{++}(\nu + \omega) + S_{i, j+1}^{\Lambda}(\omega) X_{j+1, i}^{0-}(\nu - \omega) + S_{i-1, j-1}^{\Lambda}(\omega) X_{j, i-1}^{+-}(\nu - \omega) \\ - S_{ij}^{\Lambda}(\omega) X_{ij}^{00}(\nu - \omega) + S_{i+1, j}^{\Lambda}(\omega) X_{i+1, j}^{0-}(\nu - \omega) + S_{i, j-1}^{\Lambda}(\omega) X_{ji}^{0-*}(\nu - \omega) + S_{i-1, j}^{\Lambda}(\omega) X_{i, j}^{0-*}(\nu - \omega) \\ - S_{i-1, j+1}^{\Lambda}(\omega) X_{i-1, j}^{++}(\nu - \omega) + S_{i+1, j-1}^{\Lambda}(\omega) X_{i, j-1}^{++*}(\nu - \omega) + S_{i+1, j+1}^{\Lambda}(\omega) X_{i+1, j}^{+-}(\nu - \omega). \end{aligned} \quad (22)$$

Concerning initial conditions, the single-particle contributions  $U_j n_j$  and  $U_{j+1} n_j$  in (1) are the boundary condition for  $\Sigma^{\infty}$ . However, the flow from  $\Lambda = \infty$  to finite but large  $\Lambda_i$  can be integrated analytically [17]. Effectively, by using Eq. (3), the initial conditions at the start of the numerically integrated flow at  $\Lambda_i$  read  $U_{\Pi, \Xi, \Delta}^{\Lambda_i} = 0$  and  $\Sigma^{\Lambda_i} = 0$ .

In the zero temperature case that we are interested in exclusively,  $\omega$  is continuous. We find for the single-scale

propagator and its product with  $G^{\Lambda}$  [17, 23]

$$S^{\Lambda}(\omega) = \delta(|\omega| - \Lambda) \tilde{G}^{\Lambda}(\omega) \quad (23)$$

$$S^{\Lambda}(\omega) G^{\Lambda}(\nu) = \delta(|\omega| - \Lambda) \Theta(|\nu| - \Lambda) \tilde{G}^{\Lambda}(\omega) \tilde{G}^{\Lambda}(\nu) \quad (24)$$

where  $\Theta(x)$  is a unit-step function with  $\Theta(0) = 1/2$  and  $\tilde{G}^{\Lambda}(\omega) = [G_0^{-1}(\omega) - \Sigma^{\Lambda}(\omega)]^{-1}$ . The  $\delta$ -function conveniently cancels the frequency integral  $T \sum_{\omega} \rightarrow \frac{1}{2\pi} \int_{-\infty}^{\infty} d\omega$  so that we are left with sums of the form  $\sum_{\omega=\pm\Lambda}$ .

To summarize, our fRG-2 scheme for the spinless fermion model (1) consists of a solution of the system of differential equations (17) to (22) with the replacements (23) and (24) appropriate for  $T = 0$  and the boundary conditions discussed above. We remark that our fRG-2 scheme can be derived as a special case from the more general scheme in Ref. [14] which was set up for range- $L$  correlations and spinful models. In particular, one would have to project the flow eqs. (29) and (33) in Ref. [14] to a single spin component, let  $L = 1$  and neglect any feedback between vertices.

*Details of numerical implementation.* On the technical level, our numerical code makes extensive use of fast matrix-matrix and matrix-vector multiplications to evaluate the right hand side of the flow equations. We used a Runge-Kutta integration routine and discretize the continuous Matsubara frequencies on a geometric grid with  $\mathcal{O}(100)$  points ranging from  $\omega_{min} = \mathcal{O}(10^{-6}t)$  to  $\omega_{max} = \mathcal{O}(1000t) \simeq \Lambda_i$  (in units of typical hopping  $t$ ). We avoid negative Matsubara frequencies by using time-reversal symmetry for vertices and self-energies. Linear interpolation between grid-point data is used on the right-hand side of the flow equations. With these choices, we are able to integrate the flow equations for systems consisting of  $\mathcal{O}(100)$  interacting sites on a standard desktop computer within a few hours.

Due to the complexity of the flow equations, we have performed tests against exact diagonalization (ED) for small systems (with constant  $U_j = U$ ). We compared single particle ground state expectation values  $\langle c_i^\dagger c_j \rangle$  and confirmed  $\langle c_i^\dagger c_j \rangle_{FRG} - \langle c_i^\dagger c_j \rangle_{ED} = \mathcal{O}(U^3)$  consistent with the claim that our fRG scheme is correct up to second order. Here,

$$\begin{aligned} \langle c_i^\dagger c_j \rangle_{FRG} &= \frac{1}{2\pi} \int_{-\infty}^{\infty} d\omega e^{i\omega\eta} G_{ij}^{\Lambda=0}(\omega) \\ &= \frac{1}{2} \delta_{ij} + \frac{1}{2\pi} \int_{-\Lambda_i}^{\Lambda_i} d\omega G_{ij}^{\Lambda=0}(\omega), \end{aligned} \quad (25)$$

where in the second step the large- $\omega$  tails of the Greens function have been treated analytically to produce the leading term in the last line.

It is possible to go beyond the second order scheme presented above without increasing the complexity of the presented vertex structures. For this, one can feed back parts of  $U_{\Pi,\Xi,\Delta}^\Lambda(0)$  on the right-hand side of Eqs. (4) to (6) that resemble the spatial index structure of  $v$ , see Ref. [13]. However, implementing this partial feedback procedure favoring only nearest-neighbor interactions, we observed no systematic improvement in comparison to various reference data from exact diagonalization. Consequently, we discard this feedback option in the following.

*Application: Conductance across abrupt junctions.* We now turn to an application demonstrating the perfor-

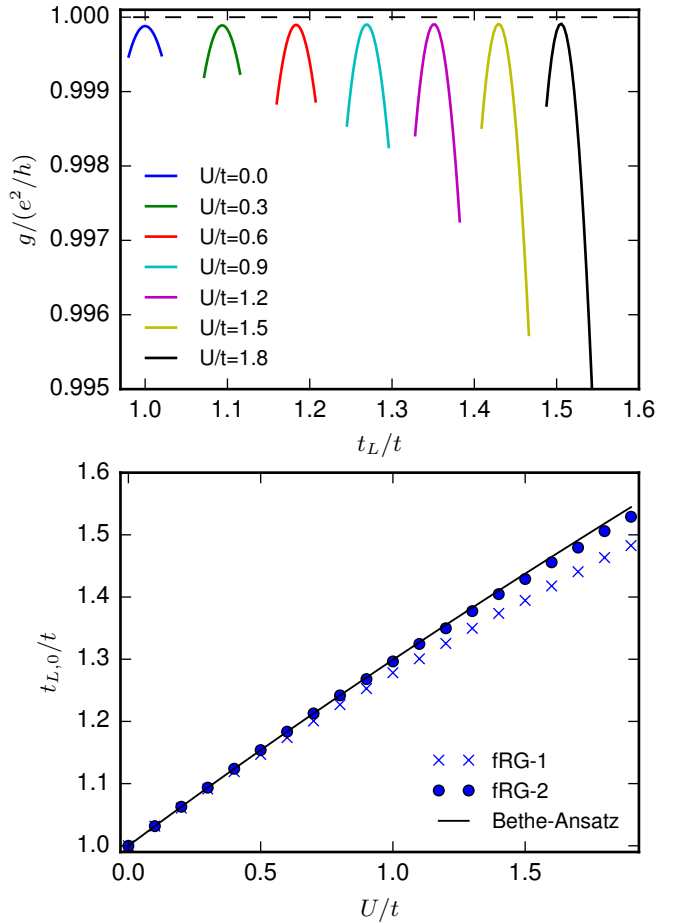


Figure 1. Top panel: Conductance  $g$  across an interacting region of length  $L = 120$  of a spinless fermion model (Eq. (1) with  $t_j = t$  and  $U_j = U$ ) connected to non-interacting leads characterized by hoppings  $t_L$  as simulated with fRG-2. Various  $U$ , increasing from left to right, are depicted. Bottom panel: The conductance maxima for different  $U$  occur at values  $t_{L,0}^{fRG-2}$  (dots) that nicely agree with the analytical predictions based on Luttinger liquid theory from Eq. (27) (solid line). Analogous results from fRG-1 are shown as crosses.

mance of the above fRG-2 scheme for spinless fermions. Whereas corresponding first order schemes (or variants thereof including a subset of higher order terms) have been employed to demonstrate Luttinger liquid physics by reproducing analytically known power laws which manifest for very large systems of  $\mathcal{O}(10^5)$  sites [10], the objectives for the second order scheme must be different due to the inherent limitation on system sizes (we will investigate power laws in momentum space in the next section).

We apply the fRG-2 scheme to a transport setup where the  $t_j$  and  $U_j$  in Eq. (1) are adjusted to form an interacting region of length  $L$  [modeled with  $U_j = U > 0$  for  $j = 0, \dots, L-2$ ] which is abruptly connected to non-interacting leads on the left and right site (with  $U_j = 0$  for  $j < 0$  or  $j > L-2$ ). The hopping strength in the

interacting region is set to  $t_j = t$ . In the leads and their connections to the interacting region, it is taken to be  $t_L$ . Generically, backscattering occurs in such a situation at the abrupt contacts and completely suppresses transport through a Luttinger liquid in the zero-temperature, infinite-system limit. One would expect that transport is only possible if the abrupt junction is turned into a smooth adiabatic one (with a then perfect conductance  $g = e^2/h$ ) by changing the values of  $t_j$  and  $U_j$  gradually with  $j$  [11]. However, it was analytically predicted by Sedlmayr et al. in Refs. [24, 25] that backscattering can also be avoided in abrupt junctions if the velocity of the elementary (bulk-)excitations match across the two connected regions (see also [26] for related ideas). For a homogeneous system as in Eq. (1) with  $t_j = t$  and  $U_j = U$ , the velocity (for  $|U| < 2t$ ) is known to be [22],

$$u = t\pi \frac{\sqrt{1 - U^2/4t^2}}{\arccos(U/2t)} \quad (26)$$

from the Bethe-Ansatz solution. Accordingly, we expect perfect conductance for given  $t, U$  once  $t_L$  is tuned to

$$t_{L,0}^{Bethe} = t\sqrt{1 - U^2/4t^2} / \arccos(U/2t). \quad (27)$$

This analytical prediction has only recently been tested numerically in Ref. [27] on the basis of a numerical conductance computation: Using a Monte-Carlo simulation the conductance  $g$  across a single junction was calculated as a function of  $t_L$ . However, since the numerical method was plagued with large error bars on the resulting conductances, a clear determination of the  $t_L$  at which a maximum of  $g$  resulted was impossible (see Fig. 7 in Ref. [27]), and only a consistency check was achieved.

In the following we show that the fRG-2 scheme is well-suited to check the above prediction and give solid numerical evidence for its validity. We implement the transport setup described above for  $L = 120$  and calculate the conductance via  $g = 4\frac{e^2}{h}t_L^2 |G_{0,L-1}^R(0)|^2$  [28] from the retarded Green function  $G^R$ . Note that at  $T = 0$ , this expression for  $g$  is exact since vertex corrections are absent [29]. In the fRG formalism, the semi-infinite leads can be taken into account analytically by adding local

self-energy terms  $\Sigma_{j,j}(i\omega) = \frac{1}{2} \left( i\omega - i\sqrt{4t_L^2 + \omega^2} \right)$  for  $\omega > 0$  to the sites  $j = 0$  and  $j = L - 1$  [28].

The conductance  $g(t_L)$  as a function of the hopping  $t_L$  in the leads is shown in Fig. 1 (top). One can clearly identify maxima at  $t_L \equiv t_{L,0}^{fRG-2}$ ; these values are extracted and plotted vs.  $U$  in the bottom panel (dots). Our results closely match the analytical prediction  $t_{L,0}^{Bethe}$  defined via Eq. (27) (solid line) except at the largest  $U$ . We have checked that while the value of the conductance maximum increases towards unity with increasing  $L$ , its position  $t_{L,0}^{fRG-2}$  does not change. Moreover, the crosses in Fig. 1 (bottom) denote the corresponding results of a first order fRG-1 calculation (using Eq. (3) with the bare interaction only) showing larger deviations from the Bethe-Ansatz value for large  $U$ .

### III. FRG IN K-SPACE

*fRG flow equations.* We now devise a second-order fRG scheme in momentum space. Our testbed will be the translational invariant spinless fermion chain at half-filling, defined by letting  $t_j = t$  and  $U_j = U$  in Hamiltonian (1). After a Fourier transformation in the spatial index of the fermion operators  $c_j = \int_k c_k e^{ikj}$  (with  $\int_k \equiv \frac{1}{2\pi} \int_{-\pi}^{\pi} dk$ ), we obtain for the non-interacting part  $H_0 = \int_k c_k^\dagger H_0(k) c_k$  with

$$H_0(k) = -2t \cos(k), \quad (28)$$

and the bare interaction vertex reads [30]

$$v(k'_1, k'_2; k_1, k_2) = \bar{\delta}_{k'_1 + k'_2 - k_1 - k_2} 2U (\cos[k'_1 - k_1] - \cos[k'_2 - k_1]), \quad (29)$$

where  $\bar{\delta}_{k'_1 + k'_2 - k_1 - k_2}$  implies conservation of crystal momentum up to integer multiples of  $2\pi$ . The flow equations simplify compared to Sec. II due to the Green functions being diagonal in momentum. For the self-energy  $\Sigma^\Lambda$  one finds

$$\partial_\Lambda \Sigma^\Lambda \left( \begin{matrix} k_1 \\ \omega_1 \end{matrix} \right) = - \int_q \int_\omega S^\Lambda \left( \begin{matrix} q \\ \omega \end{matrix} \right) U^\Lambda \left( \begin{matrix} q & k_1 & q \\ \omega & \omega_1 & \omega \end{matrix} \right), \quad (30)$$

and the 2-particle vertex  $U^\Lambda$ , in a truncation neglecting the 3-particle vertex, flows according to

$$\begin{aligned}
\partial_\Lambda U^\Lambda \left( \begin{array}{c} k'_1 \quad k'_2; \quad k_1 \\ \omega'_1 \quad \omega'_2; \quad \omega_1 \end{array} \right) = \\
+ \int_q \int_\omega G^\Lambda \left( \begin{array}{c} q \\ \omega \end{array} \right) S^\Lambda \left( \begin{array}{c} |k'| \\ \omega' \end{array} \right) U^\Lambda \left( \begin{array}{c} q \quad |k'|; \quad k_1 \\ \omega \quad \omega'; \quad \omega_1 \end{array} \right) U^\Lambda \left( \begin{array}{c} k'_1 \quad k'_2; \quad q \\ \omega'_1 \quad \omega'_2; \quad \omega \end{array} \right) \\
+ \int_q \int_\omega [G^\Lambda \left( \begin{array}{c} q \\ \omega \end{array} \right) S^\Lambda \left( \begin{array}{c} |k''| \\ \omega'' \end{array} \right) + S^\Lambda \left( \begin{array}{c} q \\ \omega \end{array} \right) G^\Lambda \left( \begin{array}{c} |k''| \\ \omega'' \end{array} \right)] U^\Lambda \left( \begin{array}{c} k'_1 \quad |k''|; \quad q \\ \omega'_1 \quad \omega''; \quad \omega \end{array} \right) U^\Lambda \left( \begin{array}{c} q \quad k'_2; \quad k_1 \\ \omega \quad \omega'_2; \quad \omega_1 \end{array} \right) \\
- \{ \omega'_1 \leftrightarrow \omega'_2, k'_1 \leftrightarrow k'_2 \}
\end{aligned} \tag{31}$$

where  $k' = k'_1 + k'_2 - q$ ,  $k'' = q + k'_2 - k_1$  and analogously for Matsubara frequencies  $\omega' = \omega'_1 + \omega'_2 - \omega$ ,  $\omega'' = \omega + \omega'_2 - \omega_1$ . Further,  $|k|$  denotes the projection of  $k$  to the first Brillouin zone (BZ)  $[-\pi, +\pi)$ . We reduced the arguments of the vertex functions to three momenta and frequencies by virtue of the momentum and frequency conserving delta-functions. For the momenta, note that if we fix  $k'_1, k'_2, k_1 \in [-\pi, +\pi)$  in the first BZ, there is no ambiguity in the choice of  $k_2 \in [-\pi, +\pi)$  fulfilling crystal momentum conservation. We again switch from fermionic to bosonic Matsubara frequencies  $\Pi, \Xi, \Delta$  as above in Eqs. (9) to (11).

*fRG-2 scheme, general form.* As before, the general flow equations (30) and (31) cannot be solved in practice, and we need to devise further approximations. The second-order approach which is equivalent to the one used in the real space scheme amounts to replacing  $U^\Lambda \rightarrow v$  on the right hand side of Eq. (31). This yields a flowing vertex of the form

$$U^\Lambda \left( \begin{array}{c} k'_1 \quad k'_2; \quad k_1 \\ \Pi \quad \Xi; \quad \Delta \end{array} \right) = v(k'_1, k'_2; k_1) + U_\Pi^\Lambda (\Pi; k'_1 \quad k'_2; k_1) + U_\Xi^\Lambda (\Xi; k'_1 \quad k'_2; k_1) + U_\Delta^\Lambda (\Delta; k'_1 \quad k'_2; k_1). \tag{32}$$

As in the real space scheme in Sec. II, the flow of the three terms  $U_\Pi^\Lambda$ ,  $U_\Xi^\Lambda$  and  $U_\Delta^\Lambda$  can be defined by the first, second and third line of the vertex flow equation with  $U^\Lambda \rightarrow v$  on the right hand side, respectively.

Instead of stopping here (as we did in the real space scheme), we want to take advantage of the simplifying assumption of translational invariance to devise a meaningful feedback scheme. Note that a full feedback of  $U^\Lambda$  would yield a vertex that depends on frequencies in a generic fashion and thus spoils the simple frequency structure of Eq. (32). Although the parametrization of the vertex  $U^\Lambda$  using three frequency variables was implemented for zero-dimensional models like the single-impurity Anderson model in Ref. [17], the need for a dense grid of  $k$  points in the vicinity of the Fermi points  $k_F = \pm\pi/2$  requires a reduction of the vertex complexity in the frequency variables to ensure applicability. Here, while sticking to the form (32) as an *Ansatz* for  $U^\Lambda$  [13, 17], we observe that it consistently allows for a feedback of its static part  $U_{(0)}^\Lambda$ , specifically

$$U_{(0)}^\Lambda = U_0 + U_\Pi^\Lambda (\Pi = 0) + U_\Xi^\Lambda (\Xi = 0) + U_\Delta^\Lambda (\Delta = 0). \tag{33}$$

Thus, a full feedback is established in terms of the vertex momentum dependence and is completely absent for the frequency dependence. This choice is partially motivated by analogy to the structure of the bare vertex, which has a nontrivial momentum- but trivial frequency dependence. On the other hand, it turns out that a feedback of the spatial features of the vertex is both necessary and sufficient to capture the phase transition to the charge-density wave long-range ordered phase for  $U > 2t$  [31]. With the feedback (33), the flow equations in the  $T = 0$  Matsubara cutoff scheme read

$$\partial_\Lambda \Sigma^\Lambda \left( \begin{array}{c} k_1 \\ \omega_1 \end{array} \right) = -\frac{\sum_{\Omega=\pm\Lambda}}{(2\pi)} \int_q \tilde{G}^\Lambda \left( \begin{array}{c} k \\ \Omega \end{array} \right) [U_0 + U_\Pi^\Lambda (\omega_1 + \Omega) + U_\Xi^\Lambda (\omega_1 - \Omega) + U_\Delta^\Lambda (0)] \left( \begin{array}{c} q \quad k_1; \quad q \end{array} \right) \tag{34}$$

$$\partial_\Lambda U_\Pi^\Lambda (\Pi; k'_1 \quad k'_2; k_1) = \frac{\sum_{\Omega=\pm\Lambda}}{(2\pi)} \int_q \theta_\Lambda (\Omega + \Pi) \tilde{G}^\Lambda \left( \begin{array}{c} q \\ \Omega + \Pi \end{array} \right) \tilde{G}^\Lambda \left( \begin{array}{c} |k'| \\ -\Omega \end{array} \right) U_{(0)}^\Lambda (k'_1 \quad k'_2; q) U_{(0)}^\Lambda (q \quad |k'|; k_1) \tag{35}$$

$$\begin{aligned}
\partial_\Lambda U_\Xi^\Lambda (\Xi; k'_1 \quad k'_2; k_1) = & \frac{\sum_{\Omega=\pm\Lambda}}{(2\pi)} \int_q \left[ \theta_\Lambda (\Omega - \Xi) \tilde{G}^\Lambda \left( \begin{array}{c} q \\ \Omega - \Xi \end{array} \right) \tilde{G}^\Lambda \left( \begin{array}{c} |k''| \\ \Omega \end{array} \right) + \theta_\Lambda (\Omega + \Xi) \tilde{G}^\Lambda \left( \begin{array}{c} q \\ \Omega \end{array} \right) \tilde{G}^\Lambda \left( \begin{array}{c} |k''| \\ \Omega + \Xi \end{array} \right) \right] \\
& \times U_{(0)}^\Lambda (q \quad k'_2; k_1) U_{(0)}^\Lambda (k'_1 \quad |k''|; q)
\end{aligned} \tag{36}$$

where  $\theta_\Lambda (\Omega) \equiv \Theta(|\Omega| - \Lambda)$  and  $\partial_\Lambda U_\Xi^\Lambda (\nu; k'_1 \quad k'_2; k_1) = -\partial_\Lambda U_\Delta^\Lambda (\nu; k'_2 \quad k'_1; k_1)$ . As in Sec. II, the initial conditions are  $\Sigma^{\Lambda_i} = 0$  and  $U_{\Pi, \Xi, \Delta}^{\Lambda_i} = 0$ . We emphasize that in terms of perturbation theory, the solution of these flow equations is correct to second order in the bare interaction  $U$ ; the  $k$ -space fRG proposed belongs to the class fRG-2, regardless of the chosen feedback scheme. Also note that the equations presented in this section describe the flow of any translationally-invariant 1d system. The specific choice of (1) only enters during the evaluation of  $\tilde{G}^\Lambda$  as well as in the initial condition.

---

*Details of numerical implementation.* Before we turn to the presentation of results, let us describe some main technical aspects of the numerical implementation.

tion of our fRG scheme. As in Sec. II, we use time-reversal symmetry to relate vertices at negative Matsubara frequencies  $-\omega$  to positive  $\omega$ ,  $U_{\Omega}^{\Lambda}(\omega; k_1' k_2'; k_1) = U_{\Omega}^{\Lambda}(-\omega; -k_1' -k_2'; -k_1)^*$  for  $\Omega \in \{\Pi, X, D\}$  and the Matsubara frequencies are discretized on a grid as in Sec. II. Similarly, the momenta are discretized with logarithmic precision around the Fermi points with distances  $\delta k_n = a^n \delta k_{min}$ , with minimal distance  $\delta k_{min} = 0.02$  and  $a = 1.5$ . Towards  $k = \pm\pi$  and  $k = 0$  the grid blends towards linear spacing. Finally, for the remaining  $q$ -integrals on the right hand side of the flow equation, we work with trapezoidal numerical integration on a  $q$ -grid similar (but much finer) than the  $k$ -grid with highest resolution at the points where the Green functions peak.

On the right hand side of the flow equations, vertices and self-energies need to be computed on generic values of frequencies and momenta that do not coincide with values on the grid. In these cases, linear interpolation between the nearest two grid frequencies and momenta is used. We can use further symmetries of the translational invariant model to reduce the computational effort. Besides time-reversal mentioned above, the model features inversion and particle-hole symmetry. The latter symmetry shuffles momenta (i.e. it moves the omitted  $k_2$  momentum) and thus the particle-hole transformed set of momenta generically is not on the grid. We thus combine this symmetry with complex conjugation (and inversion symmetry) to find

$$U^{\Lambda} \begin{pmatrix} k_1' & k_2' & k_1 \\ \Pi & X & \Delta \end{pmatrix} = U^{\Lambda*} \begin{pmatrix} |k_1' + \pi| & |k_2' + \pi| & |k_1 + \pi| \\ \Pi & X & \Delta \end{pmatrix}$$

compatible with the chosen grid points. Together with inversion symmetry, the full, say  $k_1$ -dependence of  $U^{\Lambda}$  can be reproduced from the knowledge of its  $k_1$ -dependence in one fourth of the BZ, say  $k_1 \in [-\pi, -\pi/2]$ .

During the numerical integration of the flow equations for the model (1), we observe a divergence in the interaction vertex  $U_{\Xi}(\omega_{min}, 0, \pi, 0)$  (as well as in all symmetry-related terms) once the cutoff parameter  $\Lambda$  becomes much smaller than the smallest Matsubara frequency  $\omega_{min}$ . This component describes scattering processes far away from the Fermi surface and we suspect the cause of the divergence to lie in the van-Hove singularity of the density of states at the points  $k = 0, \pi$ . This is corroborated by the observation that in the absence of both interaction and self-energy feedback, the flow equation (36) evaluated at  $(0; 0, \pi, 0)$  is governed by a term

$$\text{Re} \frac{1}{i\Lambda + 2t \cos(q)} \frac{1}{i\Lambda + 2t \cos(q + \pi)}, \quad (37)$$

which diverges for  $\Lambda \rightarrow 0$ . Moreover, the flow is regularized by any terms which open a gap in the single-particle spectrum (e.g., dimerized hoppings). Since an exact solution of (1) does not feature any divergent scattering processes, their occurrence in Eq. (36) is an artefact of the

second-order fRG flow equations (similar artefacts appear in quantum dots with many degenerate levels [32]); this is unsettling on general grounds. Pragmatically, we cut off the divergence by stopping the flow at the smallest positive Matsubara frequency,  $\Lambda^f = \omega_{min} \ll t$ . Since the divergent process is a high-energy one, this generally does not influence our results (see below for further discussions).

*Application: Occupation numbers.* The low energy theory of the homogeneous model (1) for  $|U| < 2t$  is a Luttinger liquid [22]. The fRG has a history of studying various observables and correlation functions in microscopic models for Luttinger liquids with impurities or disorder that lead to power law behavior with respect to a spatial variable, see [1, 10, 11]. The corresponding power law exponents are functions of the Luttinger liquid parameter  $K$  that is known from the Bethe-Ansatz solution,  $K = \frac{\pi}{2 \arccos(-U/2t)}$ . It was shown that a fRG-1 scheme is capable to correctly reproduce the power law exponents to first order in  $U$ . We now investigate if our fRG-2 scheme can reproduce a power law with an exponent  $\alpha$  of second order in  $U$ ,  $\alpha(U) = \mathcal{O}(U^2)$ . Specifically, we investigate the zero-temperature occupation number  $n_k = \langle c_k^\dagger c_k \rangle$  for  $k$  in the vicinity of the Fermi points which, as hallmark of Luttinger liquid physics, for  $k \rightarrow k_F$  asymptotically features a power law [22]

$$|n_k - 1/2| \propto |k - k_F|^\alpha \quad (38)$$

with

$$\alpha = \frac{K}{2} + \frac{1}{2K} - 1. \quad (39)$$

The exact  $n_k$  for our microscopic model has been calculated with DMRG in Ref. [33]. We take these data for comparison to our fRG-2 results.

We compute the occupation number  $n_k$  from the Green function  $G_k^{\Lambda^f}(\omega)$  analogous to Eq. (25). The results for  $U/t = \pm 1$  are shown in Fig. 2. In the top panel, the fRG data (dots) show reasonable agreement with the DMRG data from Ref. [33] (solid lines) in the momentum range considered. To answer the question if the asymptotic power law form (38) is captured in the fRG data, we plot a discrete log-log-derivative in the bottom panel. Indeed, the data in an intermediate  $k$ -range is compatible with the exponent in Eq. (39) (dotted lines). In contrast, simple second order perturbation theory (dash-dotted line) not only predicts the same  $n_k$  for  $U/t = \pm 1$  but asymptotically yields a logarithmic behavior for  $n_k$ . Accordingly, this is signaled by a constant simple log-derivative, which is not compatible the fRG-2 data (at least not for  $U/t = -1$ ). The fact that fRG-2 calculations yield a power law in  $n_k$  is consistent with the results of Ref. [15] where a simpler second-order scheme was used to analyze quasi-particle weights.

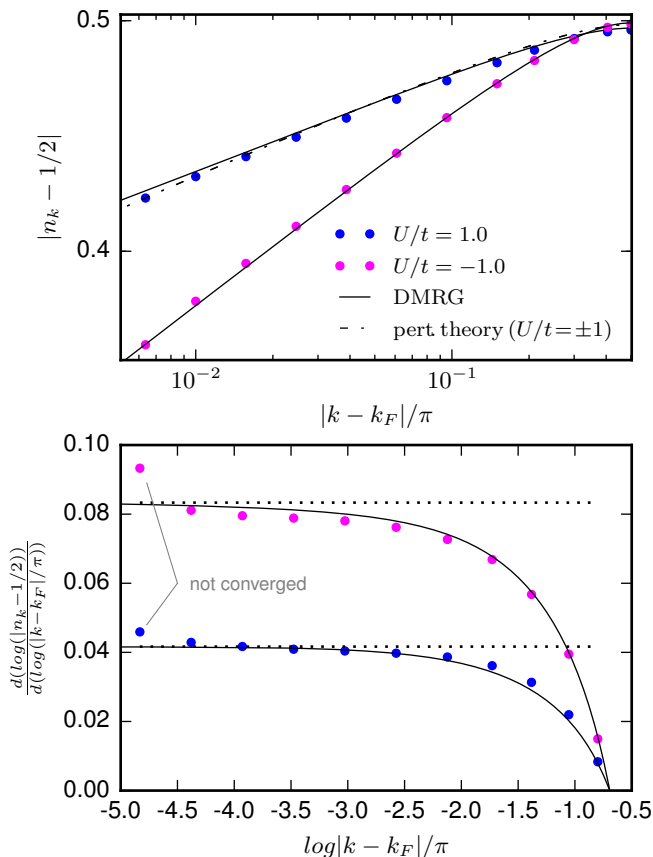


Figure 2. The top panel shows fRG results for the occupation numbers  $n_k$  of a translationally-invariant system in the vicinity of the Fermi momentum for  $U/t = \pm 1$ . The solid lines show DMRG results from Ref. [33] and the dash-dotted lines denote the results of 2nd order perturbation theory (which coincide for  $U/t = \pm 1$ ). To check if the fRG captures the power law nature of  $n_k$ , in the bottom panel, we plot a log-log derivative of the data from the top panel with asymptotic values of the Bethe ansatz exponent from Luttinger liquid theory denoted by horizontal dashed lines that is also approached by the fRG data.

More solid evidence for power laws from fRG with correct exponents would require  $k$ -data points closer to  $k_F$ . However, as can be inferred from the data in Fig. 2, instabilities occur for  $|k - k_F|/\pi < 10^{-2}$ . These instabilities close to the Fermi points are sensitive to almost all discretization parameters discussed above. Despite an extensive exploration of parameter space and alternative grid choices, no sense of convergence has been found. We suspect that this has to do with the gapless nature of the free dispersion and corresponding divergences in the Greens functions on the right hand side of the flow equations in the limit  $\Lambda \rightarrow 0$  (c.f. discussion above). Let us note that also changing to a momentum space cutoff scheme does not cure the mentioned stability problems.

## IV. CONCLUSION

In conclusion, we have formulated a fRG scheme for spinless fermions in one spatial dimension and thermal equilibrium that is correct up to 2nd order in the interaction. We have considered both a real space scheme for inhomogeneous systems and a momentum space scheme for homogeneous systems. The latter allowed for a full feedback of spatial vertex dependence in the flow equations and can be applied to any translationally-invariant model. We have devised physical test scenarios to benchmark both schemes in the realm of  $T = 0$  physics. On the upside, our fRG results compared well with known analytic solutions and outperform both perturbation theory in general and existing fRG schemes that are only correct up to first order in the interaction. On the downside, our fRG approach is correct *only to second order*, and including higher terms seems futile. Moreover, the momentum-space approach suffers from unphysical instabilities in gapless systems.

For future work, we remark that the real space formalism can easily be extended to include on-site potentials. Then the spinless fermion model is a standard model to study the intriguing physics of many-body localization. However, for this application, properties of excited states have to be accessed. Another conceivable future application would be the study of quantum phase diagrams. More general types of interaction like a next-nearest-neighbor term  $U'$  can be readily included. Likewise, more general one-dimensional dispersions can be studied with only minor modifications. In particular, interacting symmetry protected topological phases are a promising candidate for the application of fRG [34].

## V. ACKNOWLEDGMENT

We acknowledge useful discussions with Jan von Delft, Christian Klöckner, Lisa Markhof, Volker Meden and Jesko Sirker. Numerical computations were done on the HPC cluster of Fachbereich Physik at FU Berlin. Financial support was granted by the Deutsche Forschungsgemeinschaft through the Emmy Noether program (KA 3360/2-1).

- 
- [1] W. Metzner, M. Salmhofer, C. Honerkamp, V. Meden, and K. Schönhammer, Rev. Mod. Phys. **84**, 299 (2012).
  - [2] P. Kopietz, L. Bartosch, and F. Schütz, *Introduction to the Functional Renormalization Group* (Springer, 2010).
  - [3] S. G. Jakobs, V. Meden, and H. Schoeller, Phys. Rev. Lett. **99**, 150603 (2007).
  - [4] C. Karrasch, S. Andergassen, M. Pletyukhov, D. Schuricht, L. Borda, V. Meden, and H. Schoeller, Europhys. Lett. **90**, 300003 (2010).



- [5] L. M. Sieberer, M. Buchhold, and S. Diehl, Rep. Prog. Phys. **79**, 96001 (2016).
- [6] U. Schollwöck, Annals of Physics **326**, 96 (2011).
- [7] V. Meden, S. Andergassen, W. Metzner, U. Schollwöck, and K. Schönhammer, Europhys. Lett. **64**, 769 (2003).
- [8] T. Enss, V. Meden, S. Andergassen, X. Barnabé-Thériault, W. Metzner, and K. Schönhammer, Phys. Rev. B **71**, 155401 (2005).
- [9] V. Meden, W. Metzner, U. Schollwöck, and K. Schönhammer, Phys. Rev. B **65**, 45318 (2002).
- [10] S. Andergassen, T. Enss, V. Meden, W. Metzner, U. Schollwöck, and K. Schönhammer, Phys. Rev. B **70**, 75102 (2004).
- [11] C. Karrasch and J. E. Moore, Phys. Rev. B **92**, 115108 (2015).
- [12] F. Bauer, J. Heyer, E. Schubert, D. Borowsky, D. Taubert, B. Bruognolo, D. Schuh, W. Wegscheider, J. von Delft, and S. Ludwig, Nature **501**, 73 (2013).
- [13] F. Bauer, J. Heyder, and J. von Delft, Phys. Rev. B **89**, 45128 (2014).
- [14] L. Weidinger, F. Bauer, and J. von Delft, Phys. Rev. B **95**, 35122 (2017).
- [15] C. Honerkamp and M. Salmhofer, Phys. Rev. B **67**, 174504 (2003).
- [16] K. M. Tam, S. W. Tsai, and D. K. Campbell, Phys. Rev. Lett. **96**, 036408 (2006).
- [17] C. Karrasch, R. Hedden, R. Peters, T. Pruschke, K. Schönhammer, and V. Meden, J. Phys.: Condens. Matter **20**, 345205 (2008).
- [18] C. J. Halboth and W. Metzner, Phys. Rev. B **61**, 7364 (2000).
- [19] C. Honerkamp and M. Salmhofer, Phys. Rev. B **64**, 184516 (2001).
- [20] M. Salmhofer, C. Honerkamp, W. Metzner, and O. Lauscher, Prog. Theor. Phys. **112**, 943 (2004).
- [21] R. Gersch, C. Honerkamp, D. Rohe, and W. Metzner, Eur. Phys. J. B **48**, 349 (2005).
- [22] T. Giamarchi, *Quantum physics in one dimension* (Oxford University Press, 2003).
- [23] T. R. Morris, Int. J. Mod. Phys. A **09**, 2411 (1994).
- [24] N. Sedlmayr, J. Ohst, I. Affleck, J. Sirker, and S. Eggert, Phys. Rev. B **86**, 121302(R) (2012).
- [25] N. Sedlmayr, D. Morath, J. Sirker, S. Eggert, and I. Affleck, Phys. Rev. B **89**, 45133 (2014).
- [26] K. Janzen, V. Meden, and K. Schönhammer, Phys. Rev. B **74**, 85301 (2006).
- [27] D. Morath, N. Sedlmayr, J. Sirker, and S. Eggert, Phys. Rev. B **94**, 115162 (2016).
- [28] C. Karrasch, Thesis (2010).
- [29] A. Oguri, J. Phys. Soc. Jpn. **70**, 2666 (2001).
- [30] R. Shankar, Rev. Mod. Phys. **66**, 129 (1994).
- [31] L. Markhof, B. Sbierski, V. Meden, and C. Karrasch, (*in preparation*).
- [32] C. Karrasch, T. Hecht, A. Weichselbaum, Y. Oreg, J. von Delft, and V. Meden, Phys. Rev. Lett. **98**, 186802 (2007).
- [33] C. Karrasch and J. E. Moore, Phys. Rev. B **86**, 155156 (2012).
- [34] B. Sbierski and C. Karrasch, (*in preparation*).